Role of hydrogen interaction in two-dimensional molecular packing with strong molecule-substrate bonding

V. Langlais, X. Torrelles, Y. Gauthier, and M. De Santis
Laboratoire de Cristallographie, CNRS, Boîte Postal 166 X, 38 042 Grenoble Cedex 9, France
Departament de Física, Universitat Autónoma de Barcelona, 08193 Bellaterra, Spain
Institut de Ciencia de Materials de Barcelona, CSIC-Campus de la UAB, 08193 Bellaterra, Spain
(Received 7 March 2007; revised manuscript received 18 May 2007; published 26 July 2007)

Calixarene molecules deposited on Au(110) self-organize giving rise to a (19×6) coincidence cell with the substrate. Using grazing incidence x-ray diffraction, the structure has been completely resolved: gold reconstructs with a (1×3) missing-row structure while the molecules form a $(19/6\times6)$ surface cell containing two molecules. This study opens perspectives to create long-range ordered molecular templates to be used as receptors for other species providing an example of collaborative self-arrangement through a metallic substrate acting as guide and molecular flexibility.

DOI: 10.1103/PhysRevB.76.035433 PACS number(s): 68.55.−a, 61.10.Nz, 05.65.+b

Organic molecules modified with specific substituents designed for molecular recognition, allow us to build-up, "on demand," interfaces and/or surfaces with peculiar sensing, electronic, magnetic, or optical properties.[1–3] Calixarenes are known for their properties as receptors/sensors for ions, neutral species, clusters, and molecules[4,5] which make them ideal candidates to elaborate complex systems for molecular recognition.[6–8] Up to date, the main applications of calixarenes are their use as sensors and supramolecular receptor designs. They have been, for example, used as ion-selective electrodes in electrolyte-insulator semiconductors (EIS) and ion-selective-field effect transistors (ISFETs) type sensors. Some studies report on their use for the treatment of nuclear waste acting as a trap for uranium ions. Here, the main idea is to integrate these molecules into a 2D solid state environment by depositing them in a controlled fashion onto metallic surfaces and to use the resulting well-ordered molecular arrays as templates to build magnetic nanoarrays. Nevertheless, tuning the properties of such molecular surfaces requires a perfect knowledge of adsorbate-metal interactions and, first of all, of the details of the atomic/molecular arrangement. Upon deposition on most metallic surfaces, large organic molecules generally imply large coincidence unit cells, low symmetry and weak response to surface probes, making the structural details often difficult to decipher. Grazing incidence x-ray diffraction (GIXRD) can be seen as an ideal tool to solve the surface ordering of molecules on metallic substrates, nevertheless only few experiments[9–11] have been reported because organic molecules are light scatterers and the structural factors ratio of a high Z metal to that of an organic layer is, *a priori*, highly unfavorable. Solving the structure of organic molecules is thus a challenge of primary importance for a real breakthrough towards a controlled production of molecular films with designed properties. Herein, we report on the structure of a molecular film, namely, calix[4]arene, adsorbed on Au(110) surface. Au(110) offers a (1×2) missing row reconstruction that might play the role of rails to promote the molecular ordering, together with adequate reactivity properties that favor charge transfer between molecules and substrate. The high sensitivity of the measured GIXRD data has permitted (1) not only a full characterization of large organic molecules films, including H atoms but also (2) to identify the various contributions to the registry of the molecules with respect to the substrate and (3) to establish the stacking mechanisms of the molecules via dispersion forces responsible of their final configuration. Indeed, the H-H intermolecular dispersion forces play a crucial role in the molecule conformation while improving the two dimensional (2D) molecular stacking. Each molecule binds to its four nearest neighbors through 10 H-H Van der Waals bonds with an average bond distance of ~2.8 Å. Moreover, calixarenes bind to the substrate via six C-Au bonds that force two phenol cycles to lie parallel to the {111} facets of the (1×3) missing row (MR) valleys. Identifying the different contributions to the final arrangement and determining the details of the molecule configuration will help, via a better description of dispersion forces, to improve the density functional theory (DFT) calculations that are known to fail in large molecular systems.[12]

EXPERIMENTAL SECTION

The experiment was performed on the BM32 beam line at the ESRF. The surface, oriented with an accuracy better than 0.1°, was mounted in an ultrahigh vacuum (UHV) chamber (base pressure $\sim1\times10^{-10}$ mbar) coupled with a six-circle diffractometer operating in the Z-axis mode and equipped with evaporators, ion gun, and Auger spectroscopy as described elsewhere.[13] In order to increase the surface sensitivity, the incidence angle of the impinging 19 keV x rays was selected close to the critical angle (0.35°). The Au(110) surface is described by lattice vectors $(\mathbf{A}_1,\mathbf{A}_2,\mathbf{A}_3)$ along the [1-10], [001], and [110] directions, respectively, with $A_1=A_3=a_0/\sqrt{2}$, $A_2=a_0$ (bulk lattice constant=4.078 Å). The sample was prepared in UHV by standard sputtering and annealing cycles and its cleanness was checked by Auger spectroscopy. The clean surface exhibits the expected (1×2) missing row surface reconstruction reconstructed with terraces ~2000 Å wide. The calix[4]arene (purity 98%) film coverage was monitored by recording, during deposition, the intensity of one reflection, characteristic of the self-organized

molecular layer. The actual coverage was derived from the quantitative GIXRD analysis. The deposition rate was set to 0.2 ± 0.04 monolayer (ML) per minute and various substrate temperatures, from 340 to 410 ± 20 K, were tested. Upon calix[4]arene adsorption, the (1×2) missing row reflections disappeared while new reflections appeared coming from two new periodicities on the surface: (i) a (1×3) missing row from the gold substrate induced by the interaction with the molecule and (ii) a $(19/6\times6)$ periodicity exclusively due to the molecular ordering of the calixarenes. The $(12/19,0,0.1)$ reflection was followed during the deposition and intensity appears on this spot after 3.5 min, whatever the substrate temperature, and its intensity increases abruptly to saturate after ~5 min, at 1 ML completion. In the explored range of temperature, the reflection was found to sharpen with increasing temperature. However, further annealing does not improve and the $(12/19,0,0.1)$ spot disappears beyond ~500 K. The 410 K grown film was then cooled down to room temperature for data acquisition.

EXPERIMENTAL RESULTS

A previous scanning tunneling microscopy (STM) and low energy electron diffraction (LEED) study[14] showed that calixarenes yield a (3.15×6) superstructure with two distorted molecules per unit cell, while the substrate periodicity switches from (1×2) to (1×3). The surface calixarene unit cell size was found to be (9.1 Å $\times$ 24.48 Å $\pm$ 0.2 Å) and submolecular resolution allows imaging each phenol ring indicating that the molecules are adsorbed via their lower rim.[14]

The present GIXRD experimental results reveal a $(19/6\times6)$ surface structure periodicity which can be considered as an average structure of a larger one, i.e., (19×6). The (19×6) unit cell has lattice parameters coincident with those of the substrate and thus both lattices are commensurable while the measured average cell $(19/6\times6)$ cell can be considered as an incommensurable structure. This (19×6) coincidence cell is constituted by 6 $(19/6\times6)$ subunit cells which are identical or undistinguishable between them according to the resolution of the experimental techniques we have used GIXRD, STM, and LEED [Fig. 1(a)]. The main structural difference between one subcell with its neighbors corresponds to a different distribution of the gold atoms around each calixarene molecule. From one molecule to another, this atomic gold distribution is shifted by $A_1/6$ which explains why 6 correlative $(19/6\times6)$ cells are necessary to find the same substrate environment. Due to both, the identical—or experimentally undistinguishable—molecular configuration between consecutive $(19/6\times6)$ subcells (from now and on will be called as the average structure of the (19×6) coincidence cell and considered as "pseudoincommensurable" along the [1-10] direction) and the negligible lateral distortions of the topmost surface gold atoms along the $\mathbf{A}_1$ or [1-10] direction—not enhanced by the existence of a shift between them—only $H=n^*6/19$ (n integer) reflections are present. The overall diffraction pattern is shown in Fig. 1(b).

This average superstructure contains structural information from the molecular net only since any lateral shift of Au atoms in the [1-10] direction would yield non-negligible intensities in the noninteger reflections $H=n/19$, due to the large Au atomic number ($Z=79$). Similarly, the six-fold periodicity along [001] arises from the molecular film only, because the $[m,(2n+1)/6]$ (m and n integers) reflections are missing. Therefore, we can consider two data sets which can be analyzed independently: the data set-1 only reflects the periodicity of the average $(19/6\times6)$ superstructure as it has been explained above; it exhibits a $p2gg$ symmetry and comprises 486 reflections that reduce to 177 nonequivalent ones after averaging them. The resulting agreement factor from this averaging between equivalent reflections is 15%. This symmetry is consistent with the presence of two molecules per unit cell at (0,0) and (1/2,1/2), only reflections with $(H+K=2n)$ were observed.

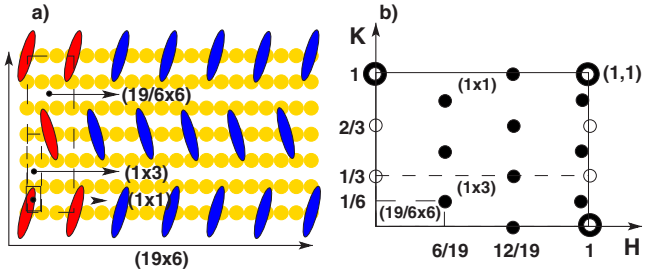

FIG. 1. (Color online) (a) Representation of the (19×6) coincidence cell formed by 6 $(19/6\times6)$ "pseudoincommensurable" cells. The (1×3) missing row as well as the (1×1) substrate periodicities are also indicated. Each colored ellipse represents one calix[4]arene molecule. (b) Schematic reciprocal space diagram of the surface corresponding to Fig. 1(a). The data set 1 and data set 2 rods are indicated as full dots and empty circles, respectively. The rectangles correspond to the calixarene (large dashed), the reconstructed substrate (short dashed), and the bulk (continuous line) unit cells.

On the other hand, the data set 2 is a combination of the (1×3) reconstructed substrate and of the coincidence (19×6) molecular film periodicity which contributes very scarcely to the intensities of these reflections. Set 2 includes 1013 reflections that reduce to 543 nonequivalent ones with the $p2mm$ symmetry, distributed along 18 fractional order rods and 4 crystal truncation rods (CTR's). The average agreement factor between equivalent reflections is in this case of 10%, a much lower value than that obtained for set 1 due to the higher intensities of this second data set. It is worth noting that the intensities of the data set 1 are, on the average, two orders of magnitude smaller than those of set 2. Moreover, from the angular width $\Delta H=2.30\times10^{-3}$ rlu of the $(0,1/3,0.1)$ reflection arising from the (1×3) missing row, we have an estimation of the terrace width of about 1000 Å (close to that of the clean surface) while the correlation length of the organic overlayer estimated from the angular widths $\Delta H=\Delta K=8.0\times10^{-3}$ rlu of the $(6/19,1/6,0.05)$ reflection is close to 700 Å.

Since both the $(19/6\times6)$ and Au(110)-(1×3) structures are commensurable along the [001] direction, the $(0,K,L)$ reflections mainly contain contributions arising from the (1×3) gold arrangement but also, in a smaller proportion, include intensity coming from the average structure of the

TABLE I. Contributions of each phase present at the surface for each family of reflections (H,K). The term S or VS means small or very small, respectively. The intensity ratio of the reflections of the (1×3) MR reconstruction and $(19/6\times6)$ cell belonging to the family $(0,n/3)$ is about a factor 50.

(H,K)	Data set classification	Types of contribution
$(0,n/3)$ ($n/3$=fractional)	Set 2	(1×3); (19/6,6)-S; (19×6)-VS
$(0,n)$ (n integer)	Set 2	(1×3); (19/6,6)-S; (19×6)-VS; (1×1)
$(n,m/3)$ (n integer; $m/3$ fractional)	Set 2	(1×3)
(n,m) ($n\neq0$, m integer)	Set 2	(1×3); (19×6)-VS; (1×1)
$(0,n/6)$ ($n/6\neq n/3$)	Set 1	(19/6,6); (19×6)-VS
$[6n/19,(2m+1)/6]$ (n,m integer)	Set 1	$(19/6\times6)$

calixarene film. To avoid a different radiation damage behavior over each measured subdata set, each data set was measured from a freshly prepared calix[4]arene surface. Both surfaces were prepared in identical conditions and their intensity evolution was followed in the same way by monitoring the (12/19,0,0.1) reflection versus deposition time. Radiation damages were checked during the whole experiment by recording periodically the intensity of several test reflections. While measuring reflections belonging to data set 1, two test reflections (6/19,3/6,0.1) and (12/19,0,0.05) were monitored at regular time intervals. The intensity decaying of these reflections after 36 h measuring corresponding to the whole period of measurements of this data set was of 25%. The intensity stability while measuring data set 2 was checked by also monitoring at regular time intervals the test reflection (0,2/3,1) intrinsic to the (1×3) missing row reconstruction. The intensity decaying of this reflection after 40 h measuring (total time invested to acquire this second data set) was of 20%. The reflections of each data set (set 1 and set 2—including CTRs) were renormalized according to the time dependence of the intensity decay obtained from their respective test reflections by using the expression: $I_{i,\mathrm{new}}(t)=I_i(t)^*I_r(t=0)/I_r(t)$, where $I_{i,\mathrm{new}}(t)$ correspond to the new intensity of reflection $I_i(t)$ measured at time t, $I_r(t=0)$ is the intensity of the test reflection at the beginning of the experiment (initial time equal to zero), and $I_r(t)$ is the extrapolated value of the intensity of the test reflection at the measuring time t. The classification of the different types of structural contributions according to the corresponding set of reflections is given in Table I.

ANALYSIS AND MODELING

The structural refinement was based on a χ^2 minimization procedure.[15] Using the data set 1, first, the shifts of the phenol groups in each molecule and their orientation were determined, the refinement being performed as follows: each molecule was considered as a rigid block and allowed to rotate around its (y,z) internal axis in Cartesian coordinates (Eulerian angles ϕ,θ,ψ defined as ϕ:$R(z)$, θ:$R(y)$, and ψ:$R(z)$, where θ and ψ were fixed by symmetry to zero,[16] and thus the internal axes of the molecule coincide with those of the unit cell). Then, one additional rotation and one translation were used for each of the two, symmetry nonequivalents, phenol rings, to account for molecular distortions: phenol-1 and phenol-2 are described by the operator $R_1(y)T_1(x,y)$ and $R_2(x)T_2(x,y)$, respectively (see Fig. 2). The corresponding rotation axes pass through the center of the phenol rings, and $R_i(x:y)$ are rotations around the x and y axes of the unit cell. T_i is a (x,y) translation of phenol-i within the $(19/6\times6)$ surface unit cell. Table II shows the initial and final (x,y,z) coordinates of the nonequivalent atoms of the molecules. The optimized parameters are thus: one scale factor, three angles [one rotation of the whole molecule ϕ around the z axis of the unit cell, one rotation of the first phenol ring $R_1(y)$, and an extra rotation for the second phenol ring $R_2(x)$], four (x,y) parameters (for both phenols translations) and two Debye-Waller (DW) factors ($B=8\pi^2\langle u^2\rangle$), one for C and H atoms and one for O atoms. The final optimized rods are displayed in Fig. 3 with a goodness-of-fit $\chi^2=1.05$. The resulting calixarene configuration is shown in Fig. 4, while the largest translation (T_1) of the first phenol ring (amplitude and orientation) is shown in Fig. 2.

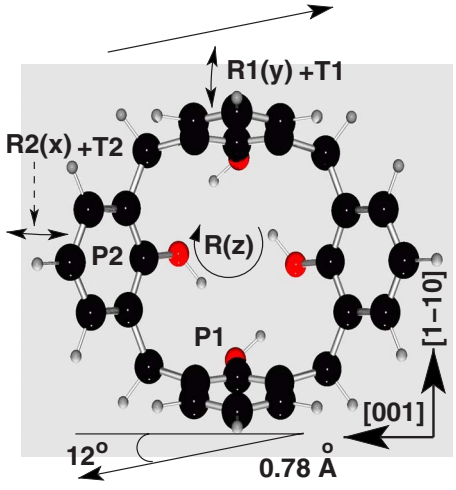

FIG. 2. (Color online) Initial configuration of the calix[4]arene molecule with the indication of the rotations and distortions applied during the fit procedure. P_1 and P_2 refer to the two nonequivalent phenol rings. $R_i(x:y)$ and T_i refer to the rotation and translation of phenol i. $R(z)(=\phi)$ means a rotation of the whole molecule around z axis. Only translation vector T_1 is indicated in the figure. For more details, see caption header of Table II. The oxygen atoms of the O-H groups are indicated in red, C atoms in black, and H atoms in gray.

TABLE II. Relative coordinates in the optimized structure: P_i-C_j refers to carbon j of phenol ring i; O_i is oxygen atom i and Au_{i-j} is the jth Au atom in layer i from the surface. Asterisks indicate fixed coordinates. The values between brackets of P_i-C_j and O_i atoms correspond to the initial (left) and final (right) coordinates of the corresponding atom. The final coordinates are obtained after applying the following rotations and translations (in relative lattice units) to the molecule: $\{R_1(y),T_1(x,y)\}=\{-13.8°,(-0.018,0.031)\}$, $\{R_2(y),T_2(x,y)\}=\{-19.1°,(-0.009,0.008)\}$ and $R(z)=-13.4°$. The error bars of y and z coordinates of Au_{i-j} atoms are (±0.001) and (±0.002), respectively. The position of the Au atoms is indicated by the shift with respect to the ideal position. The average H-H intermolecular bond length (~2.8 Å) falls within the typical range for van der Waals bonds.

Atom	x (±0.003)	y (±0.003)	z (±0.005)
P_1-C_1	(−0.325,−0.273)	(0.548, 0.585)	(−0.070,0.304)
P_1-C_2	(−0.328,−0.337)	(0.452, 0.399)	(−0.071,0.349)
P_1-C_3	(−0.318,−0.315)	(0.500, 0.491)	(−0.030,0.094)
P_1-C_4	(−0.359,−0.329)	(0.453, 0.406)	(0.387, 0.816)
P_1-C_5	(−0.376,−0.297)	(0.500, 0.500)	(0.614, 1.025)
P_1-C_6	(−0.357,−0.267)	(0.548, 0.589)	(0.387, 0.770)
O_1	(−0.286,−0.268)	(0.503, 0.545)	(−0.767,−0.346)
C_7	(−0.298,−0.340)	(0.396, 0.285)	(−0.292,0.096)
C_8	(−0.289,−0.196)	(0.603, 0.686)	(−0.303,0.086)
P_2-C_9	(0.141, 0.211)	(0.627, 0.728)	(−0.142,0.234)
P_2-C_{10}	(−0.132,−0.055)	(0.625, 0.766)	(−0.153,0.167)
P_2-C_{11}	(0.006, 0.068)	(0.608, 0.700)	(−0.326,0.080)
P_2-C_{12}	(0.136, 0.231)	(0.665, 0.824)	(0.197, 0.451)
P_2-C_{13}	(−0.132,−0.031)	(0.663, 0.862)	(0.186, 0.385)
P_2-C_{14}	(0.000, 0.111)	(0.683, 0.891)	(0.357, 0.522)
O_2	(0.016, 0.057)	(0.570, 0.051)	(−0.668,−0.137)
Au_{1-1}	0*	0*	0.000−0.106
Au_{2-1}	0.166*	0.166+0.002	−0.500−0.032
Au_{3-1}	0*	0*	−1.000−0.032
Au_{3-2}	0*	0.333+0.003	−1.000+0.024
Au_{4-1}	0.166*	0.166+0.003	−1.500−0.018
Au_{4-2}	0.166*	0.5*	−1.500+0.053
Au_{5-1}	0*	0*	−2.000−0.011
Au_{5-2}	0*	0.333+0.005	−2.000+0.009

The phenol translations in relative units are indicated in the caption header of Table II. Phenol-1 rings end up almost vertical to allow for maximum density of molecules along the [1-10] direction as shown on the top view of the calixarene arrangement (Fig. 4).

Additionally, to test the sensitivity of the experimental data to individual C and H displacements, a second optimization of the coordinates of all atoms belonging to the molecules was performed instead of optimizing the movements and distortions of groups of atoms (phenol rings). We first performed calculations, as above, including or excluding the H atoms: removing the hydrogens increases χ^2 from 1.05 to 1.5. In the next step, all nonequivalent atoms, i.e., 14 C atoms (42 xyz-positional parameters), 11 H atoms (30 xyz parameters), 2 O-atom (6 parameters) were allowed to move in addition to the molecular distortions considered in the previous section. In total 85 parameters were let free. The mean displacements (average on all directions and all atoms of a ring) off the "ideal positions" defined as those given in Table II (configuration of Fig. 4) are $|\langle\Delta C\rangle|\approx 3^*\langle\Delta C\rangle=0.074$ Å and $|\langle\Delta H\rangle|\approx 3^*\langle\Delta H\rangle=0.074$ Å for C and H, respectively. Meanwhile, χ^2 remains very close to 1 whereas the fit does not further improve with respect to that of the situation of Fig. 3. Nevertheless we note a significant decrease (by a factor 3) of the C, H, and O Debye-Waller factors compared to that of calculations where molecular distortions only are considered (see next section). In spite of the quality of the fit, the shifts of ideal positions are always smaller than the error bars and the overall picture for the molecule is thus marginally modified. In summary, while the data show good sensitivity to these parameters, the present results illustrate the fact that the methodology followed in the previous section—optimizing groups of atoms instead of all individual coordinates—is perfectly sound to extract the final configuration of the molecule.

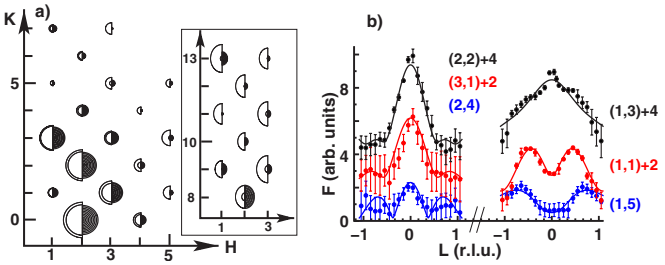

FIG. 3. (Color online) (a) The radii of the empty semicircles are proportional to the measured in-plane structure factors. The uncertainties are indicated by the two radii. The filled semicircles correspond to the structure factors calculated with the molecular model (without substrate contributions) as discussed in the text. The inset corresponds to reflections with large K values represented in this way for better clarity. (b) Selection of data set 1 rods. The numbers indicated after the reflections in brackets correspond to the applied shifts along y.

The H-C distances were fixed during the whole refinement procedure. In spite of that, experimental data showed

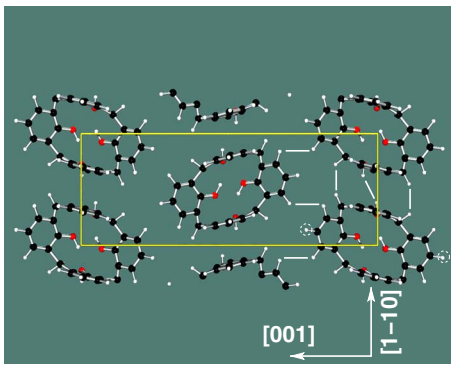

FIG. 4. (Color online) Calixarene unit cell showing the optimized phenols orientation and hydrogen bonding between neighboring molecules. Dotted circles indicate the lost hydrogens upon adsorption. Black, red, and gray colors correspond to C, O, and H atoms, respectively.

good sensitivity to H-atoms as it was proved by the worsening of fit goodness when these atoms were removed from the structure. The H-H intermolecular distances are on average close to 2.8 Å and they result exclusively from the structure refinement process. These distances correspond to van der Waals H-H bonds and the resulting interacting forces between them are expected to be small, nevertheless, they undoubtedly play a fundamental role in the stabilization of the final configuration not only of each molecule but also in the 2D molecular arrangement onto the metal surface. Recent DFT calculations performed on this system are not able to recover the final configuration of each molecule. The molecular packing in the $(19/6\times6)$ unit cell is optimized when the molecules are located at (0,0) and $(1/2,1/2)$ in the cell. Clockwise and anticlockwise rotations of one molecule with respect to the other results in a *p2gg* symmetry instead of a *c2mm* one. Even this basic configuration of the molecular packing in the unit cell cannot be retrieved when using ideal calix[4] arene molecules as those showed in Fig. 2 as an initial point to start the procedure of energy minimization of the system. The final configuration of the molecules in the unit cell depends on the interaction with their neighbors and this interaction is established in the present case via H-H intermolecular bond lengths (Fig. 4). Weak intermolecular H-H forces are usually neglected when DFT methods are applied and this omission could be the responsible of this fail when applied to organic systems. The resolved structural system we present here can supply the necessary information to advance in this field.

In the following step, we retained the initial model with two molecules per unit cell, on a (1×3) reconstructed substrate—with two rows missing in layer 1 and one in layer 2—with molecules adsorbed in the troughs. Any other model, with only two or one missing row(s), was definitely rejected on behalf of much too high goodness-of-fit criteria. The phenol groups bonding the molecule to the surface will thus sample random positions so that two adjacent nonequivalent chains will appear as equivalent for diffraction, on the average, yielding a (1×3) periodicity with *p2mm* symmetry instead of the expected (1×6) for the substrate data set 2. The full structure was then determined using a (3×3) cell made of three identical (1×3) Au surface unit cells along the *x* direction, from now on, noted as $3^*(1\times3)$ surface cell. The arrangement of the Au atoms in this $3^*(1\times3)$ cell follows the *p2mm* symmetry in agreement with the experimental data; moreover, the orientation and relative molecules separation are fixed at the values derived from step 1. Then, the calixarenes $(19/6\times6)$ unit cell was

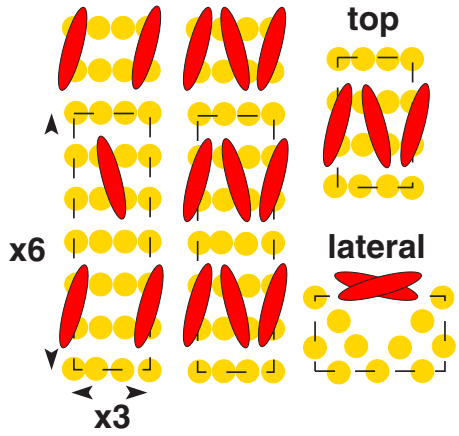

FIG. 5. (Color online) Schematic representation of the procedure we have followed to transform a $(19/6\times6)$ into an averaged $3^\star(1\times3)$ unit cell. The first step consisting on the squeezing the $(19/6\times6)$ by 5.5% along the *x* direction resulting in a (3×6) one is shown on the first left side picture. The second step corresponds to the molecular average along the sixfold period along the [001] direction. On the right hand side, resulting top and lateral views of the $3^\star(1\times3)$ cell with two molecules with 50% occupancy.

squeezed by 5.5% in the *x* direction resulting into a (3×6) one. As explained above, the six-fold period along the [001] direction was not observed in set-2 reflections, due to the (quasi) incommensurability [Fig. 1(b)]. This allows reducing the overall structure to a $3^*(1\times3)$ unit cell, when looking at the reconstructed substrate and at the film registry. Moreover, we have to account for the presence of two calixarenes in the original unit cell: both were thus located at positions $(0,1/2)$ and $(1/2,1/2)$ in the $3^*(1\times3)$ cell, with an occupancy set to 50%. Figure 5 shows in a graphical way the steps followed to reduce the $(19/6\times6)$ cell into a $3^*(1\times3)$.

In this unit cell, Au sites were allowed to relax in the *y* and *z* directions, while staying at their bulk positions along the *x* axis to maintain the actual $p(1\times3)$ substrate periodicity. The molecular layer was allowed to move in the *z* direction and seven variable Au layers were included in the fit. Thus, 1 scale factor, 18 (y,z) Au parameters, 1 *z* shift for calixarene, 3 gold DW parameters, and the occupancy of the gold top row were optimized ($\chi^2=2.5$). A selection of fractional and integer rods is plotted in Fig. 6. As usual for such MR configurations, the topmost Au row interlayer distance is contracted by about 15% while the second layer is contracted by 6%. Layer numbers 3 to 5 are relaxed by ~1% and the deepest ones (sixth and seventh) are bulklike within experimental error bars. Finally, the C/H and O DW factors are 16

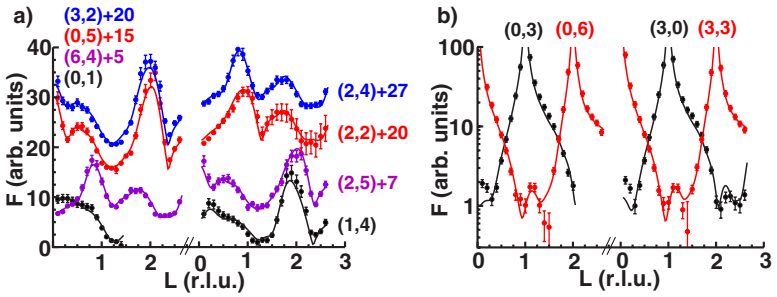

FIG. 6. (Color online) Selection of data set 2 rods. (a) Fractional order rods. The numbers correspond to curve shifts along *y* axis for better clarity. (b) CTR's in logarithmic scale. The reflections in both figures are indexed according to the $3^\star(1\times3)$ unit cell discussed in the text and in Fig. 5.

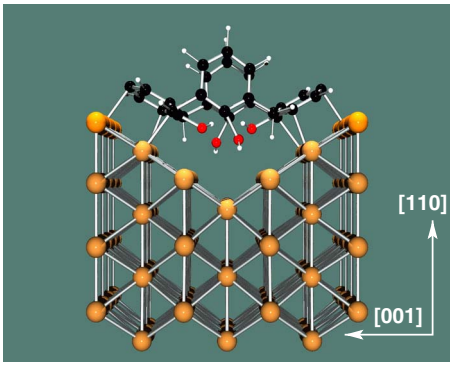

FIG. 7. (Color online) Side view of the optimized structure; calixarenes reside in the troughs with two opposite phenol almost parallel to the {111} facets. Only one calixarene molecule of the two used in the $3^{\star}(1\times3)$ unit cell is shown for clarity. Meaning of atom colors is similar to that of Fig. 4.

and 5, respectively, while the Au DW decreases continuously from 0.9 to 0.2—from surface to bulk. In spite of its relatively high value, $\chi^2(=2.5)$ is an extremely good result since the refinement was performed with a limited number of parameters as a result of the reduced $3^{*}(1\times3)$ unit cell as compared to the actual (19×6) one.

The final structure is illustrated in Fig. 7. The molecules, centered on the troughs with the OH groups pointing down the valley, are fixed to the substrate through the six Au-C bonds of the two rotated phenol rings facing the {111} facets. The attractive dispersion forces between H-atoms of neighbor molecules act as stabilizers of the molecule stacking, while internal distortions of the calixarene are due to the strong Au-C bonds. Indeed, the short bond length (average 2.27 ± 0.04 Å) matches with a calculated Au-C^{+} distance that implies a charge transfer from the molecules to the substrate.[17] Another indirect evidence of such a charge transfer is the (1×3) reconstruction that was reported upon adsorption on Au(110) of alkali and earth alkali metals accompanied by negative charge transfer towards metal.[18] Incidentally, we note that the present (1×3) reconstruction is very close to that induced by Cs adsorption that yields quite similar interlayer spacing and buckling ($\Delta d_{12}=-22\%/-15\%$, $\Delta d_{23}=-9\%/-5\%$, $b_3=0.14$ Å/0.16 Å for Cs and calixarene, respectively).[18] In addition, calculations for negatively surface charged Au(110) indicate that the (1×3) structure is favored over the (1×2).[19] Using nondistorted (as in gas phase) molecules results in a 20% larger distance to the substrate, which would imply lower interactions: as a consequence, molecular distortions can be readily assigned to the strong molecule-surface interactions assisted by charge transfer. In this case the goodness of the fit increases from $\chi^2=2.5$ to 3.5.

CONCLUSION

In summary, using GIXRD, we fully determined not only the structure of a self-organized calix[4]arene monolayer on Au(110)-(1×2) but also the forces responsible for molecular distortion and 2D organization. The substrate switches from a (1×2) to a (1×3) MR reconstruction, with a contraction of the first interlayer distance of about 15%. Conformational changes of the molecules to match the substrate corrugation are observed with two opposite—rotated—phenol rings lying almost parallel to the Au {111} facets and the other phenols almost perpendicular to the surface. The short Au-C bonding distance and the substrate structural change, implying long range mass transport, indicate a strong molecules/substrate interaction. Structural determination of large molecules deposited on metals provides clear insight to the rules governing self-organization and molecule-substrate interactions that are the driving mechanisms to build molecular templates and grow complex organic/inorganic systems.

ACKNOWLEDGMENTS

V.L. and X.T. thank the Spanish Ministry of Education and Science (M.E.y C.) for its support through the "Ramon y Cajal" program and Project No. MAT2005-01736, respectively. We acknowledge for beam time at ESRF and thank the BM32 beam line staff for technical support.

[1] S. Rösler, R. Lucklum, R. Borngräber, J. Hartmann, and P. Hauptmann, Sens. Actuators B **48**, 415 (1998).
[2] J. Park, A. N. Pasupathy, J. I. Goldsmith, A. V. Soldatov, C. Chang, Y. Yaish, J. P. Sethna, H. D. Abruña, D. C. Ralph, and P. N. McEuen, Thin Solid Films **438-439**, 457 (2003).
[3] S. M. Barlow and R. Raval, Surf. Sci. Rep. **50**, 201 (2003).
[4] R. Ferdani, L. J. Barbour, and G. W. Gokel, J. Supramol. Chem. **2**, 343 (2002).
[5] F. Davis, M. Gerber, N. Cowlam, and C. J. M. Stirling, Thin Solid Films **284-285**, 678 (1996).
[6] C. D. Gutsche, in *Calixarenes in Monographs in Supramolecular Chemistry*, edited by J. F. Stoddart (Royal Society of Chemistry, Cambridge, 1998).
[7] *Calixarenes in action*, edited by L. Mandolini and R. Ungaro (Imperial College Press, London, 2000).
[8] *Calixarenes 2001*, edited by Z. Asfari, V. Bohmer, J. Harrowfield, and J. Vicens (Kluwer Academic Publishers, Dordrecht, 2001).
[9] H. L. Meyerheim, Th. Gloege, and H. Maltor, Surf. Sci. Lett. **442**, L1029 (1999).
[10] H. L. Meyerheim and Th. Gloege, Chem. Phys. Lett. **326**, 45 (2000).
[11] T. Kidd, R. D. Aburano, H. Hong, T. Gog, and T.-C. Chiang, Surf. Sci. **397**, 185 (1998).
[12] S. Krystián and P. Pulay, Chem. Phys. Lett. **229**, 175 (1994).
[13] R. Baudoing-Savois, G. Renaud, M. De Santis, A. Barbier, O. Robach, P. Taunier, P. Jeantet, O. Ulrich, J. P. Roux, M. C. Saint-Lager, A. Barski, O. Geaymond, G. Berard, P. Dolle, M. Noblet, and A. Mougin, Nucl. Instrum. Methods Phys. Res. B

149, 213 (1999).
[14] V. A. Langlais, Y. Gauthier, H. Belkhir, and O. Maresca, Phys. Rev. B **72**, 085444 (2005).
[15] E. Vlieg, J. Appl. Crystallogr. **33**, 401 (2000).
[16] X. Torrelles, E. Barrena, C. Munuera, J. Rius, S. Ferrer, and C. Ocal, Langmuir **20**, 9396 (2004).
[17] M. Barysz and P. Pyykkö, Chem. Phys. Lett. **285**, 398 (1998).
[18] P. Häberle, P. Fenter, and T. Gustafsson, Phys. Rev. B **39**, 5810 (1989).
[19] R. Heid and K. P. Bohnen, Phys. Rep. **387**, 151 (2003).